Simulation Experiments on the Spreading Behaviour of Molten Core Melts: KATS-3b and KATS-4

G. Fieg, H. Werle, F. Huber

Institut für Neutronenphysik und Reaktortechnik
Institut für Reaktorsicherheit
Projekt Nukleare Sicherheitsforschung

Forschungszentrum Karlsruhe
Technik und Umwelt

Wissenschaftliche Berichte

FZKA 5887

Simulation Experiments on the Spreading Behaviour of Molten Core Melts: KATS-3b and KATS-4

G. Fieg, H. Werle, F Huber

Institut für Neutronenphysik und Reaktortechnik
Institut für Reaktorsicherheit
Projekt Nukleare Sicherheitsforschung

ABSTRACT

In future Light Water Rectors special devices (core catchers) might be required to prevent containment failure by basement erosion after reactor pressure vessel meltthrough during a core meltdown accident. Quick freezing of the molten core masses is desirable to reduce release of radioactivity. Several concepts of core catcher devices have been proposed based on the spreading of corium melt onto flat surfaces with subsequent water cooling.
Therefore a series of experiments to investigate high temperature melt spreading on flat surfaces has been carried out using alumina-iron thermite melts as a simulant. The oxidic and metallic phases of the melt are separated and spread on different surfaces. The influence of a shallow water layer on the surface onto the spreading behaviour has also been studied.
KATS-3b was the first dry spreading test of a series of experiments which investigate the spreading phenomena of high temperature melts. It represents the dry reference case for the following wet spreading test, KATS-4. In this report all data of KATS-3b and KATS-4 are presented which are necessary for further analysis.

Simulationsexperimente zum Ausbreitungsverhalten von Kernschmelzen: KATS-3b und KATS-4

ZUSAMMENFASSUNG

Für zukünftige Leichtwasserreaktor-Kraftwerke werden spezielle Einbauten (Kernfänger) erforderlich sein, um das Containment-Versagen infolge von Erosion des Fundamentes bei einem Kernschmelzunfall zu verhindern. Die geschmolzenen Kernmassen sollen möglichst schnell in einen festen Zustand übergeführt werden, um die Freisetzung von radioaktivem Material zu reduzieren. Einige der vorgeschlagenen Kernfängerkonzepte beruhen auf dem Prinzip, die geschmolzenen Kernmassen auf ebenen Flächen zu verteilen und anschließend mit Wasser zu kühlen.
Es wurde deshalb eine Serie von Experimenten durchgeführt, um das Ausbreiten von Schmelzen mit hoher Temperatur auf ebenen Flächen zu untersuchen. Dabei wurde als Simulationsmaterial eine Thermitschmelze aus Aluminiumoxid und Eisen verwendet. Die oxidischen und metallischen Komponenten werden dabei getrennt und auf verschiedene Ausbreitungsflächen geleitet. Der Einfluß niedriger Wasserschichten auf den Flächen auf den Ausbreitungsprozeß wurde ebenfalls untersucht.
KATS-3b war das erste trockene Ausbreitungsexperiment in einer Serie von Experimenten zur Untersuchung des Ausbreitungsverhaltens. Es stellt auch den trockenen Referenzfall für den folgenden Test KATS-4 dar, bei dem die nasse Ausbreitung untersucht wurde. In diesem Bericht sind sämtliche Daten von KATS-3b und KATS-4 zusammengefaßt, die für weitere Analysen notwendig sind.

CONTENTS

1. INTRODUCTION

Special devices (core catchers) might be required in future Light Water Reactors to prevent containment failure by basement erosion after reactor pressure vessel meltthrough during a core meltdown accident. It is desirable to cool, preferably freeze, the molten core masses quickly in order to reduce the release of radioactivity and the danger of interaction of the melt with structural materials. This implies that thin layers of corium are formed on these structures. Several concepts of core catchers have been proposed to meet these requirements [1,2,3,4].

Also the core catcher foreseen for the European Pressurized Reactor (EPR) is based on these principles [5], fig.1. The basic concept of this device is to retain the corium masses in the cavern under the reactor pressure vessel long enough to collect most of the corium inventory after the breach of the pressure vessel. Afterwards a gate opens between the cavern and a spreading compartment, into which the corium melt is released. This gate opens as a result of erosion by the melt and the time period for this process has to be about one hour, which is long enough to gather most of the corium after the breach of the pressure vessel. This time period will also allow an increase of the melt temperature and correspondingly a decrease of viscosity to assure a fast spreading of the melt. The composition of corium is ~180 tons of oxidic melt (UO_2 and ZrO_2) and ~120 tons of metallic melt (steel and Zr). Cooling of the melt is foreseen from the top by flooding the melt surface with water after the end of the spreading phase.

Corium melt spreading and subsequent interaction of spread corium with water during flooding are generic problems of the EPR core catcher and similar concepts. Models are under development to describe these phenomena. They have to be verified by experiments. The number of experiments with real molten corium will be limited; therefore, tests with appropriate simulant materials are required.

The spreading of corium onto concrete floors has been investigated theoretically [7,8]. In addition, Suzuki et al. [8] conducted several spreading experiments using stainless steel melts to verify their modeling. Moody [9] modeled the spreading of corium melt onto a flat surface with and without overlying water. The MELTSPREAD-1 code [10] has been developed at the Argonne National Laboratory and describes the spreading of melts onto dry and wet surfaces. Malinovic et. al. [11] investigated spreading of thermite melts on dry and wet concrete surfaces and also studied the quenching rates due to overlying water pools. Greene et. al. [12] studied the spreading of a variety of materials onto wet and dry surfaces to derive correlations for spreading rates and lengths.

1

At Siemens/KWU the CORFLOW code [13] has been developed for EPR core catcher investigations. This code describes the spreading of melts onto dry surfaces and has been verified by low temperature melt spreading experiments at the CORINE facility [13]. In addition, CORFLOW has to be verified with spreading experiments using higher temperature melts, and this is the main motivation for this series of experiments.

In this report two spreading experiments of a series of experiments are described which have been conducted using high temperature alumina-iron thermite melts up to 300 kg. These tests are called KATS-experiments (abbreviation for Karlsruher Ausbreitungsexperimente mit Thermit-Schmelzen, Karlsruhe spreading experiments with thermite melts). Spreading experiments of separated alumina and iron melts on dry surfaces cannot directly simulate the spreading of real corium melts. The goal of these experiments is not to simulate as close as possible the behaviour of a corium melt, but to provide experimental data to validate CORFLOW. Therefore there is no need for a realistic scaling-up of the experimental layout to meet the EPR corecatcher design features. Knowledge of material properties, especially viscosity, for both, the simulant and the real melts is essential for extrapolating the results to reactor conditions using a computer model.

2. EXPERIMENTAL SETUP

2.1 Test facility and thermite reaction

. The test rig, fig.2, consists of a large reaction crucible for thermite to generate molten alumina and iron, two containers under the crucible to gather the separated melts and the spreading areas (channels). To avoid thermal attack the crucible wall consists of a ceramic material (mainly magnesia). Fig.3 shows schematically the setup. The thermite powder (300 kg) in the crucible is heated up to 130 to 180 ^{0}C for about 24 hours before ignition to release any moisture. Thermocouples inside the thermite powder and the crucible wall control this heating-up phase. At the bottom of the crucible a nozzle, 40 mm in diameter, is installed to discharge the melt. The opening of the nozzle is performed by a pneumatic device, which is initiated by a central control unit. The thermite powder is ignited electrically at the top center of the load. The reaction time for a 300 kg load lasts about 30 s. A delay time of 10 to 15 s between the end of the thermite reaction and the release is needed to allow outgassing of the melt. The arrival of melt at the

nozzle is detected by three thermocouples which are located above the nozzle.

The specific energy of the exothermic thermite reaction $8Al +3Fe_3O_4 \rightarrow 4Al_2O_3 +9Fe$ is $3.85 \cdot 10^6$ J/kg, yielding an adiabatic melt temperature of 2600 ^{0}C. From experience it is known that only 95% of the thermite masses are reacting which reduces the melt temperature to 2450 ^{0}C. Due to wall erosion in the crucible the temperature at the time of melt release is furthermore reduced to 2200 ± 50 ^{0}C. This temperature has been calculated with the EquiTherm-Program [14]. It agrees well with measured values from temperature measurements of the jet (pyrometric method and with W/Re-thermocouples).

A load of 300 kg thermite produces 160 kg iron and 140 kg oxidic melt. The two phases of the melt, oxide and metal, separate practically immediately during the reaction and the iron melt pours firstly out of the nozzle after opening. The metallic and oxidic melts are gathered in two separate containers before spreading into the channels is initiated. The iron melt container is positioned under the nozzle outlet. Under the chosen experimental conditions the pouring takes about 8 s for the iron melt. Once the metallic melt is exhausted, the jet is guided into the second container by a movable chute. The containers are insulated with cordierite plates (52% SiO_2, 37% Al_2O_3, 6.5% MgO) with an open porosity of 23%. This material is highly resistant to temperature shocks and erosion due to high temperature melt jets. Some wall material of both containers is dissolved into the melts because of the low melt temperature of cordierite (1600 ^{0}C). Due to incomplete chemical reaction and wall erosion the composition of the oxidic melt is about as follows:

Al_2O_3	83%
FeO	6%
MgO	1.5%
SiO_2	8.5%
MnO	1%

The quality of separation of the two melt phases depends strongly on the time, when the jet is guided from the iron container into the oxide container via the movable chute. The time to move the chute is calculated under the assumption that the nozzle diameter does not increase due to material erosion. Furthermore, for a short time interval a mixture of oxidic and metallic melt may flow through the nozzle. Therefore a complete separation is not possible with this method. In the case that the jet is directed too late into the oxidic container some oxidic melt is gathered in the container for the iron melt. Except for the small resulting higher pressure head in the container the spreading of iron is not

disturbed by the presence of this oxide. Yet, in the case that the jet is directed too early in the oxide container, some iron gathers at the bottom of the oxide container and spreads onto the surface together with the oxide melt. To minimize this risk the bottom of the gate to the spreading surface is situated 2 cm above the container bottom. This swamp volume for the excess iron melt in the oxide container was 2.4 liters. It turned out that even so a full separation of the melts could not be achieved.

The gates between the containers and spreading channels are closed with ceramic plugs made of magnesia. They have a conical form with the smaller dimensions towards the container holding the melt. The reason for this conical form is to insure a safe opening at the moment when the plugs are released by a pneumatic and mechanical spring device. The gate height is 5 cm for both containers, the gate widths are somewhat smaller than the channel widths. Figures 4 and 5 show the dimensions of containers, gates and spreading channels for the iron and oxidic melts. The corresponding data are listed in Table 1. This table lists also the main parameters of the individual tests at the onset of spreading.

The channel width is 40 cm for the oxide and 20 cm for the iron. The different widths are chosen so that about the same melt layer height results for the same spreading lengths of the two melts. The spreading channel is constructed of concrete covered with cordierite plates and additionally with ceramic tiles having a water-tight surface (an alumina/silica mixture). These additional ceramic tiles are necessary for the wet spreading experiment KATS-4. The channels have been carefully adjusted with a slope of less than about 1mm over a length of 1 m against the horizontal.

The end of the channels is not blocked by a vertical wall, but consists of inclined plates (base length 10 cm, heigth 6 cm) which allow both melts to flow over and out of the channels. This special feature has been introcuded especially with respect to the wet experiment KATS-4 to reduce the risk of an energetic water-melt interaction due to water being enclosed by the hot melts.

2.2 Instrumentation

During the spreading process the temperature of the melts is measured with W-Re thermocouples at three different axial positions in the channels, with the thermocouple junction level 10 mm above the channel floor, see Table 2. Thermocouples of type K (1 mm outer diameter) are positioned at different vertical positions (5, 25, 45 and 65 mm above the floor level) at the same axial positions as the W-Re thermocouples. These thermocouples have been installed to indicate the arrival time of the melt. Fig. 6 shows the positions and identification of the single measuring points of

4

both tests, KATS-3b and KATS-4. KATS-4 is additionally equipped with pressure transducers at different axial positions. Their vertical distance from the channel floor is 0.20 m, they are mounted at the top of the channel walls.

Several video-cameras record the spreading process. In test KATS-4 with melt spreading onto wet surfaces, additionally two high speed cameras (1000 frames per second) were installed to record eventual energetic interactions between water and melt (vapour explosions).

2.3 Data Recording

The measured and amplified signals were recorded using a digital 32 channel transient recording system. In test KATS-3b a sampling rate of 1kHz per channel was applied leading to an overall recording time of 256 s. The transient recorder was started with the command to ignite the thermite powder.
After conduct of the experiment the recorded data were transferred and stored on a disk. The evaluation is done with a special computer program supplied together with the transient recording system.
In test KATS-4 the sampling rate has been increased to 10 kHz because of the additional pressure transducers. As a result the total recording time was reduced to 25.6 s. Here the transient recorder has been started with the command to open the first gate.
For synchronisation reasons of the different video recorders and high speed cameras flashlights were triggered together with the commands for thermite ignition and opening of the gates.

2.4 Control System

The commands during conduct of the tests (thermite ignition, tapping the crucible orifice, moving the chute and opening the gates) are controlled by an electronic control system. The duration for the thermite reaction and hence the tapping of the orifice has been estimated with an established rule of thumb: the reaction front velocity proceeds at 25 to 30 mm/s for the thermite powder as used in these tests. The time intervals for the iron and oxidic melt to flow out of the reaction chamber have been calculated with Torricelli's law. From this the time to move the chute leading the oxidic melt into the oxide container has been estimated. The opening of the two gates are initiated after melt release from the reaction crucible

was ended. The timing for the different commands were not identical in both tests, Table 3 shows these times for both tests.

3. EXPERIMENTAL CONDITIONS

Table 1 lists all relevant data at the onset of the experiment. The amount of thermite, dimensions of containers and the spreading channels are identical in both experiments. The only difference was the existence of a layer of 1 cm of water on the spreading surfaces in KATS-4, whereas the spreading in KATS-3b has been performed onto dry surfaces. KATS-3b with dry channels is the dry reference test for the wet spreading experiment KATS-4. The influence of shallow water levels onto the spreading mechanism was the objective of this test.

Post experimental analysis showed that the amount of iron and oxidic melts in the containers and accordingly in the spreading channels differed from theoretical preassumptions, Table 1 lists these post experiment analysis data. In case of fully separated melts 160 kg iron and 140 kg oxidic melts are expected.

The melt level heights in both containers would be 422 mm for the iron and 407 mm for the oxide under the assumption that no wall material is eroded due to thermal or chemical attack. To handle the case of an incomplete separation of the two melt phases the release gate in the oxidic container was situated 20 mm above the bottom. The resulting volume of 2.5 l under the gate level can accomodate about 16 kg of iron melt.

Post experimental analysis of test KATS-3b showed that the amount of masses in both containers at the onset of spreading differed remarkably from estimated values. There was only about 120 kg of iron melt in the iron container, 39.1 kg were found in the oxide area (4.6 kg in the container and 34.5 kg in the spreading channel). 135 kg of oxidic melt was gathered in the oxide container and about 6 kg was found in the iron container. An amount of about 1 kg oxide was found as a thin crust on top of the spread iron in the iron channel.

Taking into account these melt distributions and additionally the amount of eroded wall material inside the iron container, the melt level heights have been recalculated and are given in Table 1. The total heights in the containers amounted to be 330 mm in the iron- and 440 mm in the oxide container. Due to the 20 mm difference between bottom and gate the effective height was 420 mm in the oxide container.

4. EXPERIMENTAL RESULTS

4.1 KATS-3b

Spreading of the iron melt

Fig. 7 shows traces of three W-Re thermocouples at three axial positions (0.3 m, 1.1 m and 1.9 m, measured from the gate). The temperature close to the gate is 2180 ^{0}C which is in good agreement with the calculated value of 2177±50 ^{0}C. Further downstreams the temperature are lower, 2152 ^{0}C at 1.1 m and 2140 ^{0}C at 1.9 m. Table 4 shows the arrival times at the type K thermocouples locations. Included are also the average velocities as calculated from the thermocouple readings. Figs 8 through 11 show the corresponding transient registrations for these thermocouples. Fig. 12 shows the transient spreading of the iron melt, the three different curves correspond to thermocouples at three different vertical positions (5 mm, 25 mm and 45 mm heights). The response time of these thermocouples is about 50 ms. Any systematic errors due to this response are cancelled in evaluating leading edge velocities because time differences are used between two different thermocouple readings. Fig. 12 shows that thermocouples at higher vertical positions respond at later times than the corresponding lower ones.

The pouring rate can be calculated according to Torricelli's law including a pouring factor of 0.6 for the given geometry [15]. It starts with 10.1 l/s at the onset of opening the gate and decreases linearly to zero at 3.4 seconds. The average spreading velocity is 2.6 m/s at the beginning (between thermocouple positions 0.3 m and 1.1 m) and decreases to 2.1 m/s towards the end of the spreading channel.

Post experimental analysis showed that 12 kg of iron remained in the container, 95 kg were found on the spreading surface and 16 kg escaped at the end of the spreading channel.

Spreading of the oxide melt

The spreading of the oxide melt started 21 s after the iron spreading. Fig. 13 shows traces of three W-Re thermocouples at three axial positions (0.3 m, 1.1 m and 1.9 m, measured from the gate). The temperature close to the gate is 2160 ^{0}C, 20 K lower than the corresponding value for the iron melt. Further downstreams the temperature are lower, 2125 ^{0}C at 1.1 m and 2115 ^{0}C at 1.9 m. Table 4 shows the arrival times at the type K thermocouples locations. Included are also the average velocities

as calculated from the thermocouple readings. Figs 14 through 17 show the corresponding transient registrations for these thermocouples. Fig. 18 shows the transient spreading of the oxide melt, the three different curves correspond to thermocouples at three different vertical positions (5 mm, 25 mm and 45 mm heights). As for the iron melt, also here the thermocouple readings show that at higher vertical positions they respond at later times than the corresponding lower ones.

The pouring rate can be calculated according to Torricelli's law including again a pouring factor of 0.6 for the given geometry. It starts with 29 l/s at the onset of opening the gate and decreases linearilly to zero at 3.5 seconds. The average spreading velocity for the oxide melt is about 2.5 m/s between 0.3 and 1.1 m and 2.3 m/s between 1.1 and 1.9 m.

As already mentioned in chapter 3, due to incomplete separation of metallic and oxidic melt about 39 kg of iron melt was guided into the oxide container. Most of this iron was found below the oxidic crust in the spreading channel. Only 4.6 kg of iron has been found in the swamp below the gate which was designed to gather about 16 kg. It seems that the height of 2 cm of this swamp was too low to retain an iron melt. The post experiment examination showed an average oxidic crust thickness of 75 mm. The average porosity of this crust is about 35 %. Most of the alumina-silica ceramic tiles in the channel (23 kg) were eroded after spreading. Some of the oxidic melt has also been ejected over the inclined plate at the channel end. Table 5 shows the post experimental mass balances for both melts.

The composition of the oxidic crust has been analyzed at two positions, one inside the container and one near the end of the spreading channel. Tab.6 shows the result of this SEM analysis (with Microprobe). The composition inside the container has a low percentage of silica (9.5%). This is from partial erosion of cordierite plates from the container liner. From the amount of about 7% iron oxides it can b e deduced that about 95% of the thermite powder has reacted. The high content of silica in the spreading channel (29%) is due to the erosion of the bottom tiles. The relatively low content of magnesia (1.4%) indicates only a minor wall erosion of the reaction crucible. This is due to the existence of a relatively strong oxidic crust between the melt and the crucible magnesia liner which has been formed during former experiments.

4.2 KATS-4

As mentioned in chapter 3 the initial experimental conditions are identical to those in KATS-3b. The only difference is the presence of a layer of 1 cm water in both channels. The water temperature at the moment of filling shortly before onset of the test was 50 ^{0}C.

Spreading of the oxide melt

In test KATS-3b the iron melt has been released ahead of the oxide melt. Here the spreading started with the oxide melt. The reason was that stronger energetic interactions between water and iron melt have been anticipated than in the case of the oxide melt and water.
The water temperature in the oxide channel fell to about 30 ^{0}C at the onset of spreading. Two energetic reactions have been recorded during oxide spreading, the first one 10-20 cm from the gate opening, the second one at 1m distance. The pressure transducers recorded short pressure peaks between 0.2 and 0.3 MPa, the duration was 1-2 ms. The high speed camera recording also showed that these energetic reactions took place within less than 1 ms.
Only two of six W-Re thermocouples survived the energetic reactions, both were located in the spreading channel for the iron melt at 0.3 m and 1.9 m from the gate.
As to the K-type thermocouples, only 13 out of 24 survived the energetic reaction. Tab. 7 shows the arrival times for both melts at the thermocouple locations distributed axially and vertically in the spreading channels. The corresponding transient temperature registrations for the oxide melt are shown in figs. 19 and 20.
 The average spreading velocity for the oxidic melt is 1.7 m/s compared to 2.4 m/s in the dry case. During the two energetic reactions in the oxidic spreading channel some oxidic melt has been ejected out of the channel and the instrumentation has partly been destroyed. Some of the oxide has been ejected into the iron spreading channel. Some water also may have been ejected out of the channels during these energetic explosions.
Post experiment analysis showed that 3.5 kg of iron have been found in the container for the oxidic melt. Six individual pieces of iron ranging from 1 to 16 kg were found in the oxide spreading channel (total amount 26.7 kg). Several kg of iron have been ejected out of the iron spreading channel during the energetic iron melt/water interaction. Furthermore, there is evidence that some iron melt has been gathered in the oxide container and drained into the oxide spreading channel at the time when the gate has been opened. No conclusions can be done from this post experiment

analysis how much iron melt has been ejected from the iron channel into the spreading channel for the oxide melt and how much has been poured from the container. Tab. 8 shows the mass balance and distribution for the KATS-4 experiment.

The average crust height in the spreading channel for the oxide melt is 75 mm, similar to the result in KATS-3b. Here also some of the oxide melt was flowing over the inclined plate at the channel end. In contrary to KATS-3b none of the alumina-silica plates have been molten or eroded, which must be attributed to the presence of the water layer. Some few kilograms of oxide melt have been ejected over a distance of more than 50 m during the two energetic melt/water interactions.

Spreading of the iron melt

The water temperature in the iron melt spreading channel has been measured at the channel entrance shortly at the onset of spreading to be 70 °C. No measurement could be done further downstream because of instrument failures due to oxide melt ejection. This increase of temperature is also due the fact that oxidic melt has been ejected into the channel.

Only two of six W-Re thermocouples survived the energetic reactions, both were located in the spreading channel for the iron melt at 0.3 m and 1.9 m from the gate. The temperature of the iron melt near the gate (2170 °C, thermocouple TWE.105), fig. 21, is about the same as in the dry reference test KATS-3b (2180°C), the temperature towards the channel end (1.9 m) is somewhat lower (2040 °C). The transient temperature readings for the surviving K-type thermocouples are shown in figs.22 and 23.

One strong energetic reaction has been recorded during iron melt spreading at a distance of about 1 m from the gate with a short pressure peak of 0.4 Mpa. There the concrete wall between the two channels was partly destroyed by this last event. Melt, pieces of concrete and steel structure material have been ejected over a distance of more than 50 m. The average spreading velocity was about 1.4 m/s (Table 7).

An analysis of the energetic reactions is difficult because the amount of melt and water masses which reacted with each other are not known. The results of KATS-4 are therefore only of a qualitative nature.

Post experiment analysis has also been applied to KATS-4. 119.4 kg of iron melt (from the theoretical value 160 kg) were found on the spreading surface. The iron container was practically empty. About 5 kg of iron melt flowed over the inclined plate onto the soil. Several kg of iron melt have been ejected out of the channel during

the energetic melt/water interaction. No conclusion can be drawn from this post analysis how much iron melt has been ejected into the oxide channel. Table 8 shows the mass balance and distribution of the KATS-4 experiment. Due to melt ejection during spreading it was not possible to analyse the amount of melts in the containers at the onset of spreading.

5. SUMMARY

Dry and wet (1 cm water layer) spreading of high temperature melts were studied in KATS-3b and KATS-4, respectively. Energetic reactions of both types of melts (iron and oxide) with water during wet spreading (KATS-4) were observed causing ejection of small fractions of the melts and a decrease of the overall spreading velocity compared to dry spreading. Nevertheless in both tests the melts spreaded evenly over the available area.

6. REFERENCES

1.   J.D. Fish, M. Pilch and F. Arrellano, "Demonstration of Passively-Cooled Particle-Bed Core Retention," Proceedings of the 5th Post Accident Debris Cooling Information Exchange Meeting, Karlsruhe, Germany,28-30 June 1982, 319-324

2. H. Alsmeyer et. al., "Improved Containment Concepts for Future Large LWR's," IEA Int. Conf. Technology Responses to Global Environmental Challenges, Kyoto, Japan, 6-8 November 1991, 471-489

3. A. Turricchia, "How to Avoid Molten Core/Concrete Interaction and Steam Explosions," Proc. 2nd Organization for Economic Cooperation and Development Committee on the Safety of Nuclear Installations Specialist's Meeting on Molten Core Debris-Concrete Interaction, Karlsruhe, Germany, April 1992, KfK-Report 5108, 503-518

4.   J.M. Seiler, F. Balard, M. Durin, A. Méjane, S. Pigny and I. Szabo, "Conceptual Studies of Core Catchers for Advanced LWR's," Proc. Int. Conf. Design and Safety of Advanced Nuclear Power Plants, Tokyo, Japan, October 25-29, 1992, Vol III, p. 300-327

5. M. Michel et. Al., "EPR Safety Approach and Consideration of Severe Accidents,"Transactions of the ENC '94, Lyon, France, October 2-6,1994, Vol.II,502-506

6. M. Fischer, Siemens/KWU, private communication, May 1996

7. M.S. Kazimi, "On the Liner Failure Potential in MARK-I Boiling Reactors," Nucl. Science and Engineering, **103**, 59-69 (1989)

8. H. Suzuki, T. Mitadera, I. Sakaki and T. Zama, "Fundamental Experiment and Analysis for Melt Spreading on Concrete Floors," Proc. Intern. Conference on Nucl. Energy (ICONE-2), San Francisco, March 21-24, 1993

9. F.J. Moody, "First Order Analyses of Molten Corium Heat Transfer," ANS Proc. 1989 National Heat Transfer Conference, August 6-9, 1989, Philadelphia, PE, 217-224

10. M.T. Farmer, J.J. Sienicki, B.W. Spencer and C.C. Chen, "Status of the MELTSPREAD-1 Computer Code for the Analysis of Transient Spreading of Core Debris Melts," Proc. 2nd Organization for Economic Cooperation and Development Committee on the Safety of Nuclear Installations Specialist's Meeting on Molten Core Debris-Concrete Interaction, Karlsruhe, Germany, April 1992, KfK-Report 5108, 489-502

11.   B. Malinovic and R. E. Henry, "Experiments Relating to Drywell Shell-Core Debris Interaction", EPRI-NP 7196L (February 1991)

12. G.A. Greene, K.R. Perkins and S.A. Hodge,"Mark I Containment Drywell-Impact of Core/Concrete Interactions on Containment Integrity and Failure of the Drywell Liner," Proceedings of an International Symposium on Source Term Evaluation for Accident Conditions, Columbus,OH, October 28-November 1, 1985, pp 429, International Atomic Energy Agency, Vienna, (1986).

13.   J. M. Veteau and R. Wittmaack, "CORINE Experiments and Theoretical Modelling," FISA-95 Symposium - EU Research on Severe Accidents, Luxembourg, Nov. 20-22, 1995, 271-285

14.   M. Steinbrück, private communication

15.   Dubbel Taschenbuch für den Maschinenbau, Springer Verlag, 17. Auflage, 1990, B52-B53

Table 1 Dimensions of melt containers, spreading channels, melt heights and melt masses for KATS-3b and -4

	Unit	Iron	Oxide
Container inner width	cm	17.8	37.8
Container inner depth	cm	32.5	32.5
Release gate height	cm	5.0	5.0
Release gate width	cm	14.0	34.0
Channel width	cm	20.0	40.0
Channel length	cm	250	250
Total height of melt [1]	cm	42.0	40.7
Height of iron melt [2]	cm	29.4	4.8
Height of oxide melt [2]	cm	3.6	39.2
Total height of melt [2]	cm	33.0	44.0
Calculated oxide melt [1]	kg	0.0	140.0
Calculated iron melt [1]	kg	160.0	0.0
Actual oxide melt [2]	kg	5.8	134.8
Actual iron melt [2]	kg	120.0	39.1

[1] Data calculated under the assumption of ideal melt separation

[2] Data derived from post experimental examination

Table. 2 Location of thermocouples in tests KATS-3b and KATS-4

Iron melt				
Axial position of thermocouples (m)	Thermocouple # Vertical positions of thermocouples			
	5 mm	25 mm	45 mm	65 mm
0.3	TK.E.105 TW.E.105	TK.E.125	TK.E.145	TK.E.165
1.1	TK.E.205 TW.E.205	TK.E.225	TK.E.245	TK.E.265
1.9	TK.E.305 TW.E.305	TK.E.325	TK.E.345	TK.E.365
Oxide melt				
Axial positions of thermocouples (m)	Thermocouple # Vertical positions of thermocouples			
	5 mm	25 mm	45 mm	65 mm
0.3	TK.O.105 TW.O.105	TK.O.125	TK.O.145	TK.O.165
1.1	TK.O.205 TW.O.205	TK.O.225	TK.O.245	TK.O.265
1.9	TK.O.305 TW.O.305	TK.O.325	TK.O.345	TK.O.365

TK= K-type thermocouple
TW= C-type thermocouple
"E"=iron channel
"O"=oxide channel

Table 3 Time charts of the KATS control system for the two tests

KATS-3b	
Event	Time (s)
Ignition of thermite powder Flashlight #1 Start data recording	0
Start of melt release	45
Start of moving chute	51.01
Chute on end position *)	53.72
Start of high speed camera (iron melt)	53.82
Open gate for iron melt Flashlight #2	54.33
Start of high speed camera (oxide mellt)	74.87
Open gate for oxide melt Flashlight #3	75.38

KATS-4	
Event	Time (s)
Ignition of thermite powder Flashlight #1	0
Start of melt release	40.06
Start of moving chute	47.59
Start of high speed camera (oxide melt)	74.66
Open gate for oxide melt Flashlight #2 Start data recording	75.17
Start of high speed camera (iron mellt)	79.10
Open gate for iron melt Flashlight #3	80.22

Table 4   Arrival times of iron and oxide melts at axial and vertical thermocouple locations in test KATS-3b

Iron melt			
Axial position of thermocouples (m)	Arrival time (s) Vertical positions of thermocouples		
	5 mm	25 mm	45 mm
0.3	0.115	0.17	0.19
1.1	0.42 (2.6m/s)	0.52 (2.29m/s)	0.56 (2.16m/s)
1.9	0.80 (2.1m/s)	0.94 (1.9m/s)	0.99 (1.86m/s)

Oxide melt			
Axial positions of thermocouples (m)	Arrival time (s) Vertical positions of thermocouples		
	5 mm	25 mm	45 mm
0.3	0.16	0.18	0.2
1.1	0.48 (2.5m/s)	0.5 (2.5m/s)	0.52 (2.5m/s)
1.9	0.83 (2.28m/s)	0.83 (2.42m/s)	--

The velocities in the brackets are melt front velocities between two consecutive axial thermocouple positions.

Table 5 Mass balances of oxide and iron melts in KATS-3b

	Oxide melt (kg)	Iron melt (kg)
As calculated from thermite reaction:	140	160
Gathered in containers before melt spreading:		
Oxide container	134.8	39.1
Iron container	5.8	120.0
After melt spreading:		
Oxide container	1-2	4.6
Oxide channel	>133	34.5
Iron container	-	12
Iron channel	1-2	111

Table 6 SEM-Analysis of two oxidic KATS-3b samples

	Sample Position	
	Container (wt %)	Spreading channel (1.9 m) (wt %)
MgO	1.4	1.4
Al2O3	82.0	60.4
SiO2	9.5	29.3
MnO	1.1	1.1
FeO	6.0	7.8

Table 7 **Arrival times of iron and oxide melts at axial and vertical thermocouple locations in KATS-4**

Iron melt				
Axial position of thermocouples (m)	Arrival time (s) after gate opening Vertical positions of thermocouples			
	5 mm	25 mm	45 mm	65 mm
0.3	0.29	0.29	0.28	-
1.1	-	-	-	-
1.9	1.41 (1.43m/s)	1.65 (1.17m/s)	1.40 (1.43m/s)	1.40
Oxide melt				
Axial positions of thermocouples (m)	Arrival time (s) after gate opening Vertical positions of thermocouples			
	5 mm	25 mm	45 mm	65 mm
0.3	0.5	-	0.5	
1.1	-	-	-	-
1.9	1.45 (1.68m/s)	1.45	1.45 (1.68m/s)	1.45

The velocities in the brackets are melt front velocities calculated between the axial positions 0.3m and 1.9m

Table 8 Mass balances of oxide and iron melts in KATS-4

	Oxide melt (kg)	Iron melt (kg)
As calculated from thermite reaction:	140	160
After melt spreading:		
Oxide container	2-4	3.5
Oxide channel	≈ 120	26.7
Iron container	≈ 0	0
Iron channel	2-3	125
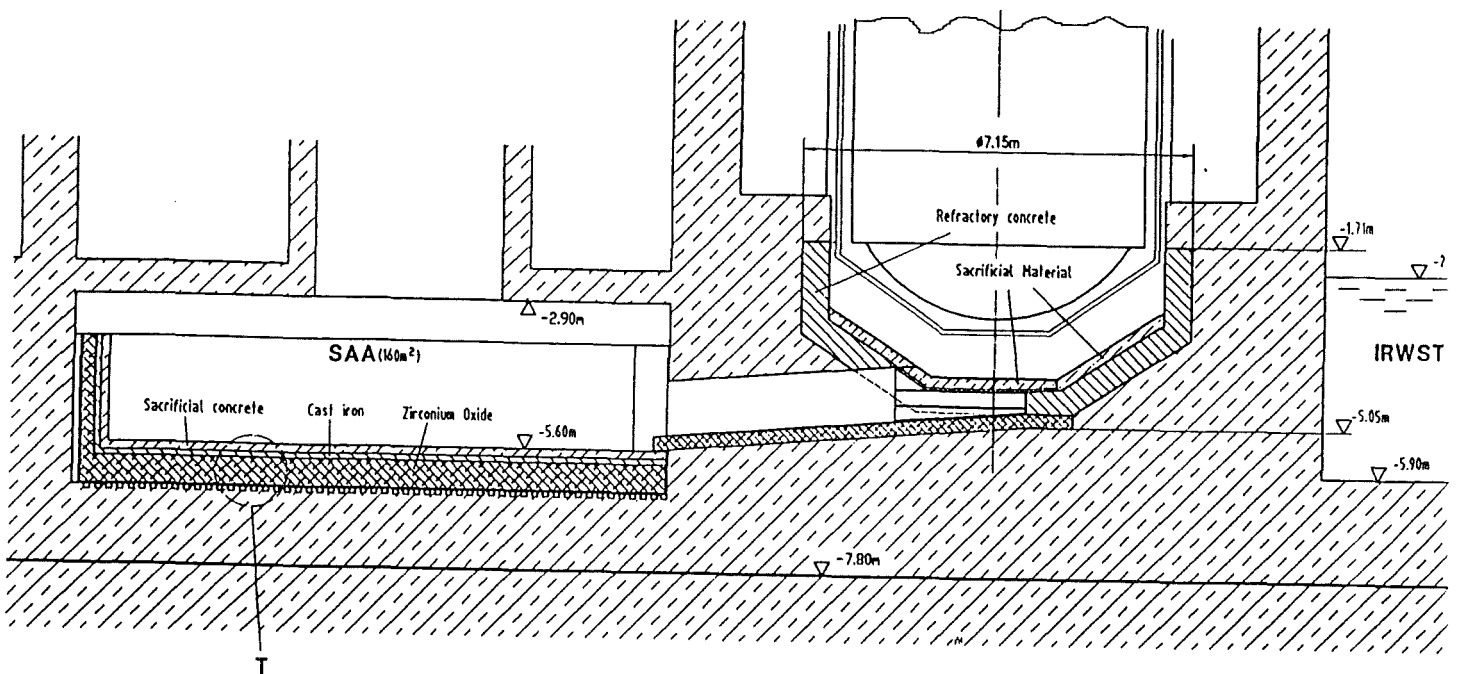
Fig. 1 Improved Reference Concept of the EPR Core-melt Retention System
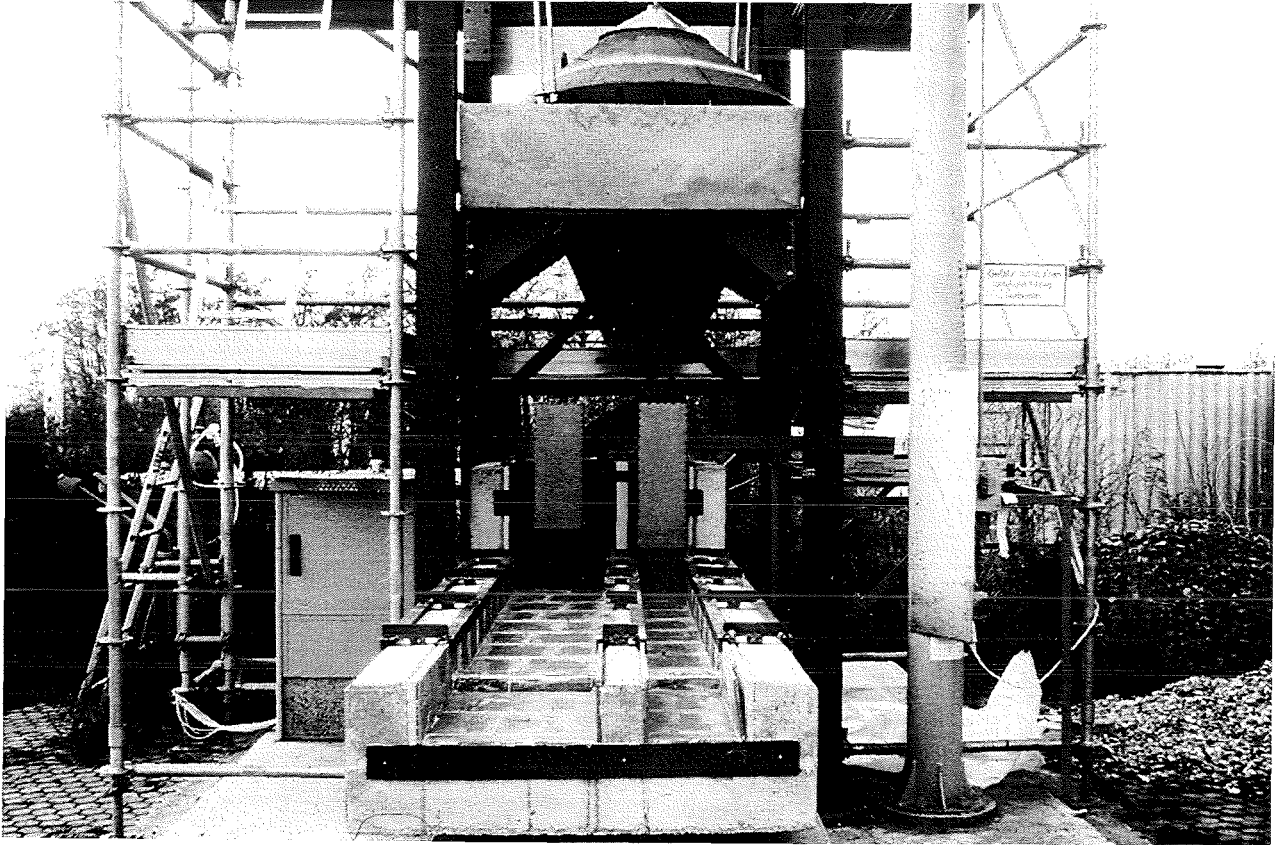
Fig.2 Photo of the KATS Facility

Thermite

Oxide melt — Reaction crucible

Iron melt

Movable chute

Tap mechanism

Iron chamber

Oxide chamber

Iron channel

Oxide channel

Release gates
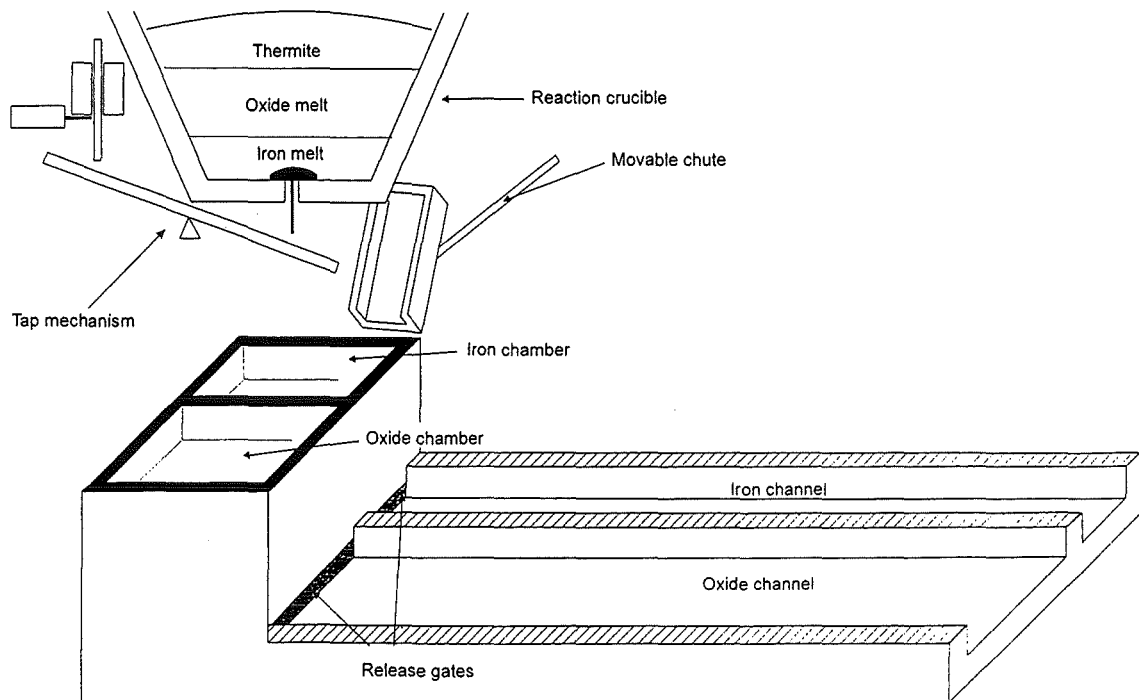
Fig.3 Schematics of the KATS Facility
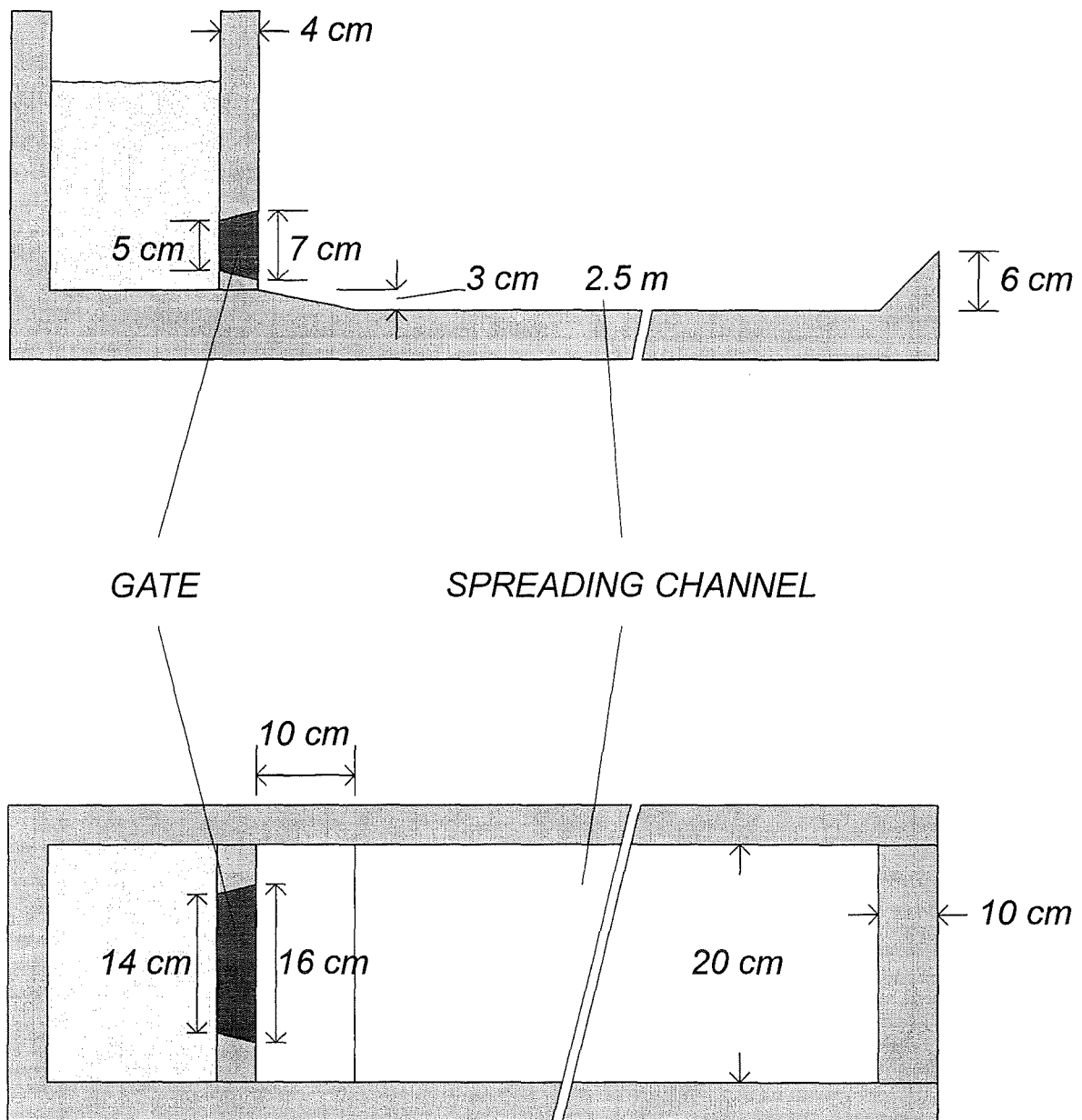
Fig. 4   Geometry and dimensions for the spreading of iron in KATS-3b and -4
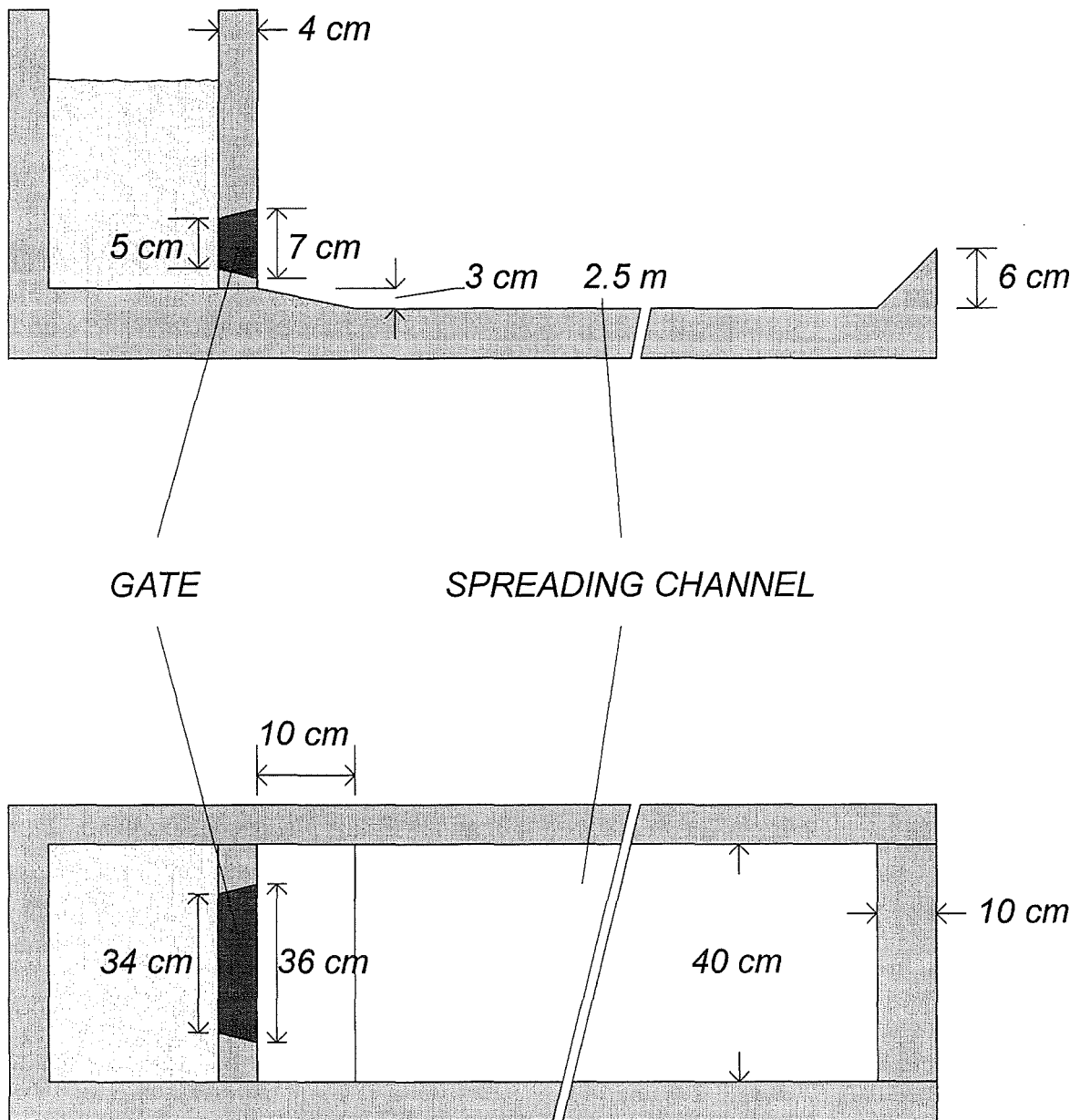
Fig. 5 **Geometry and dimensions for the spreading of oxide in KATS-3b and -4**

○ thermocouples to measure temperature
∘ thermocouples to detect the arrival of the melt

pos 1   pos 2   pos 3

iron

TW.E.105   TK.E.265   TW.E.305
TK.E.145   TK.E.245   TK.E.365
TK.E.125   TK.E.225   TK.E.345
TK.E.105   TK.E.205   TK.E.325
                        TK.E.305

flow direction ⇒

oxide

TK.O.105   TK.O.205   TK.O.305
TK.O.125   TK.O.225   TK.O.325
TK.O.145   TK.O.245   TK.O.345
            TK.O.265   TK.O.365
TW.O.105   TW.O.305

pos 1   pos 2   pos 3

| 300 | 800 | 800 |

KATS-3b

○ thermocouples to measure temperature
∘ thermocouples to detect the arrival of the melt

pos 1   PE.1   pos 2   PE.2   pos 3   PE.3

iron

TW.E.105   TK.E.265   TW.E.305
TK.E.145   TK.E.245   TK.E.365
TK.E.125   TK.E.225   TK.E.345
TK.E.105   TK.E.205   TK.E.325
                        TK.E.305

flow direction ⇒

oxide

TK.O.105   TK.O.205   TK.O.305
TK.O.125   TK.O.225   TK.O.325
TK.O.145   TK.O.245   TK.O.345
            TK.O.265   TK.O.365
TW.O.105   TW.O.305

pos 1   pos 2   pos 3
PO.1   PO.2   PO.3

| 300 | 800 | 800 | 200 |

explanation :

TK = thermocouples type K
TW = thermocouples type W
E = iron - channel
O = oxide - channel

125 = position 1 , height 25 mm

PO 1 = pressure transducer , oxide , pos. 1
PE 1 = pressure transducer , iron , pos. 1

KATS-4

Fig. 6 Locations of thermocouples and pressure transducers in both tests

Fig. 7 Test KATS-3b   Temperature of the iron melt at Pos.1/2/3

24
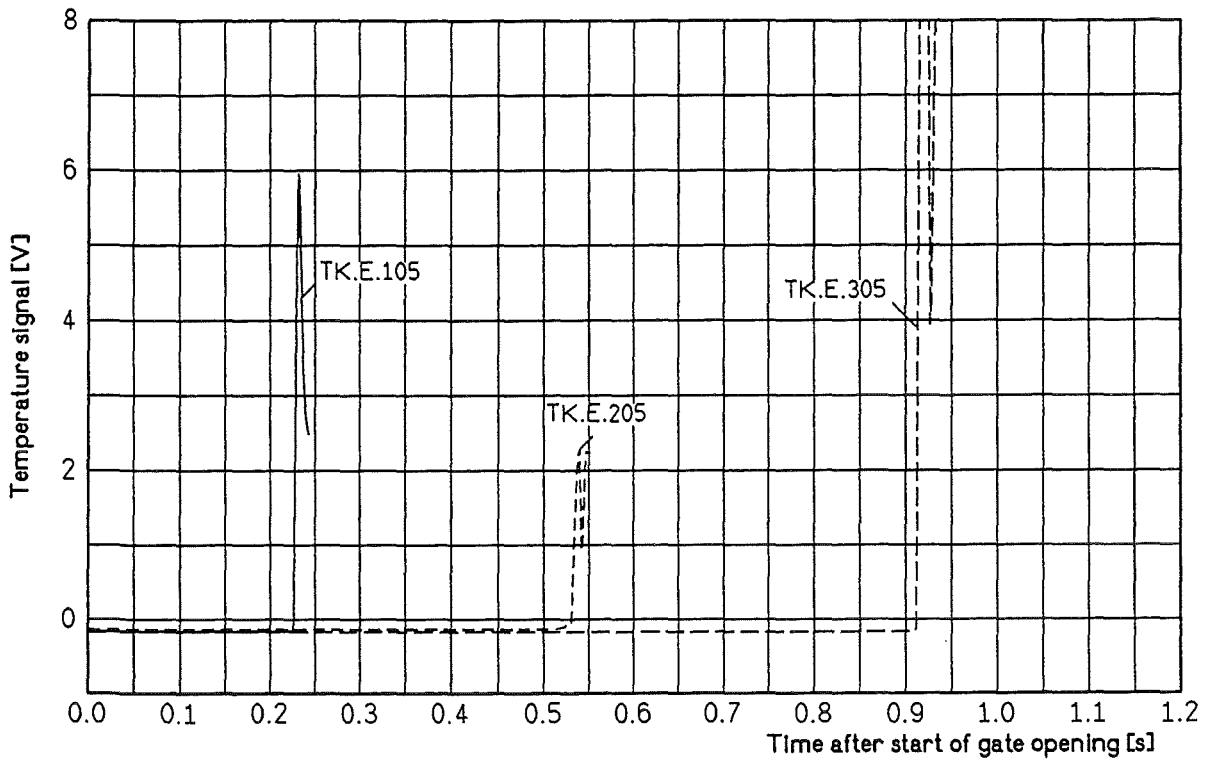
Fig. 8 Test KATS-3b   Detection of the iron melt at 5mm height
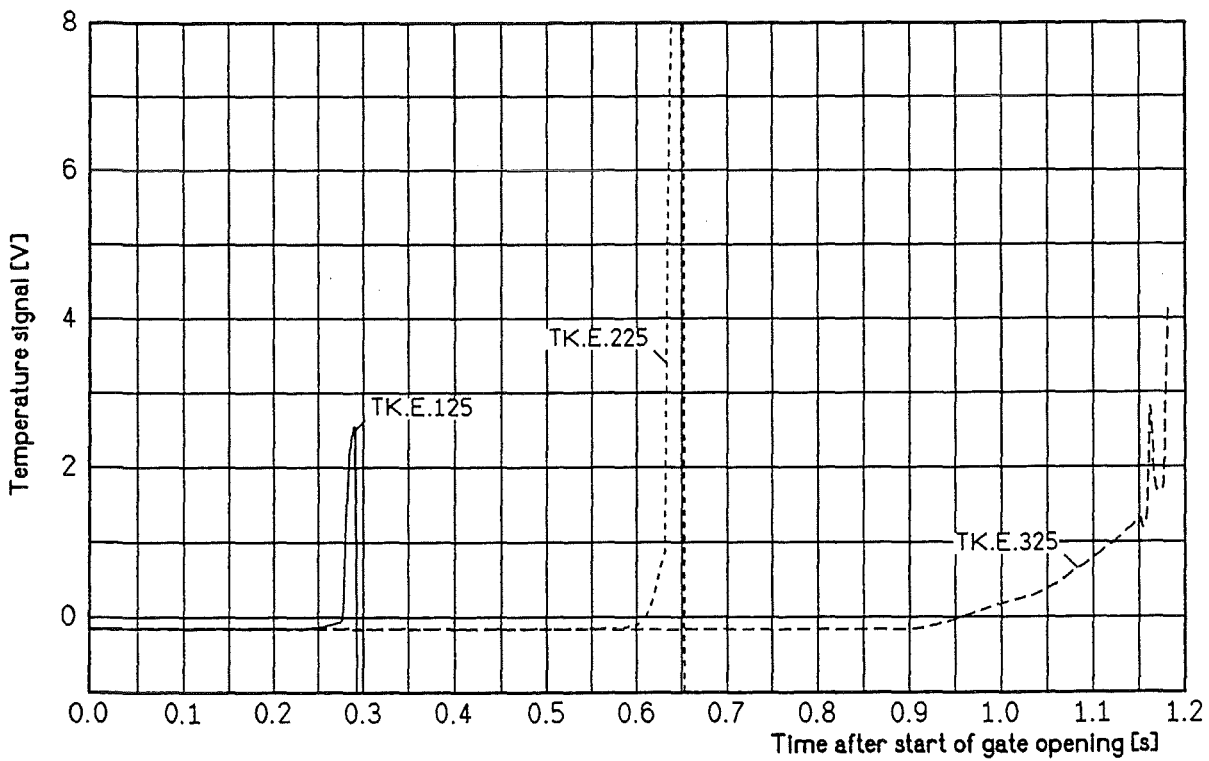
Fig. 9 Test KATS-3b   Detection of the iron melt at 25mm height

25
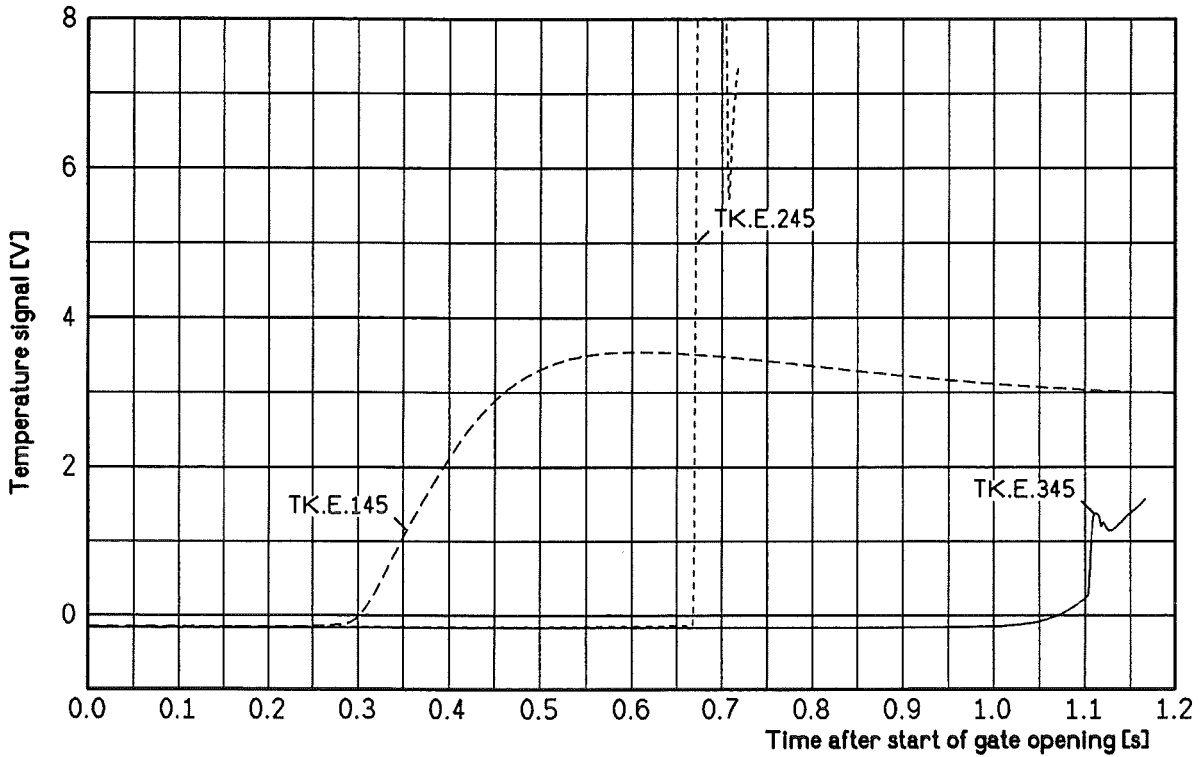
Fig. 10 Test KATS-3b   Detection of the iron melt at 45 mm height
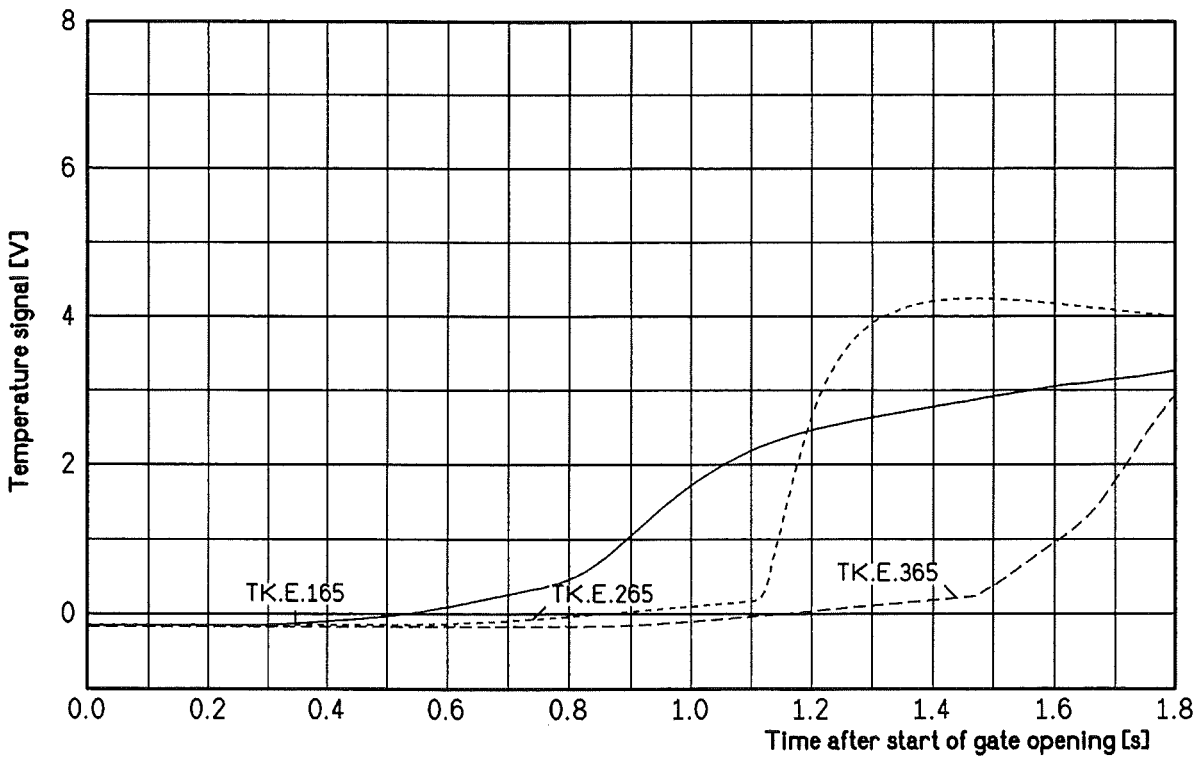
Fig.11 Test KATS-3b   Detection of the iron melt at 65 mm height

26
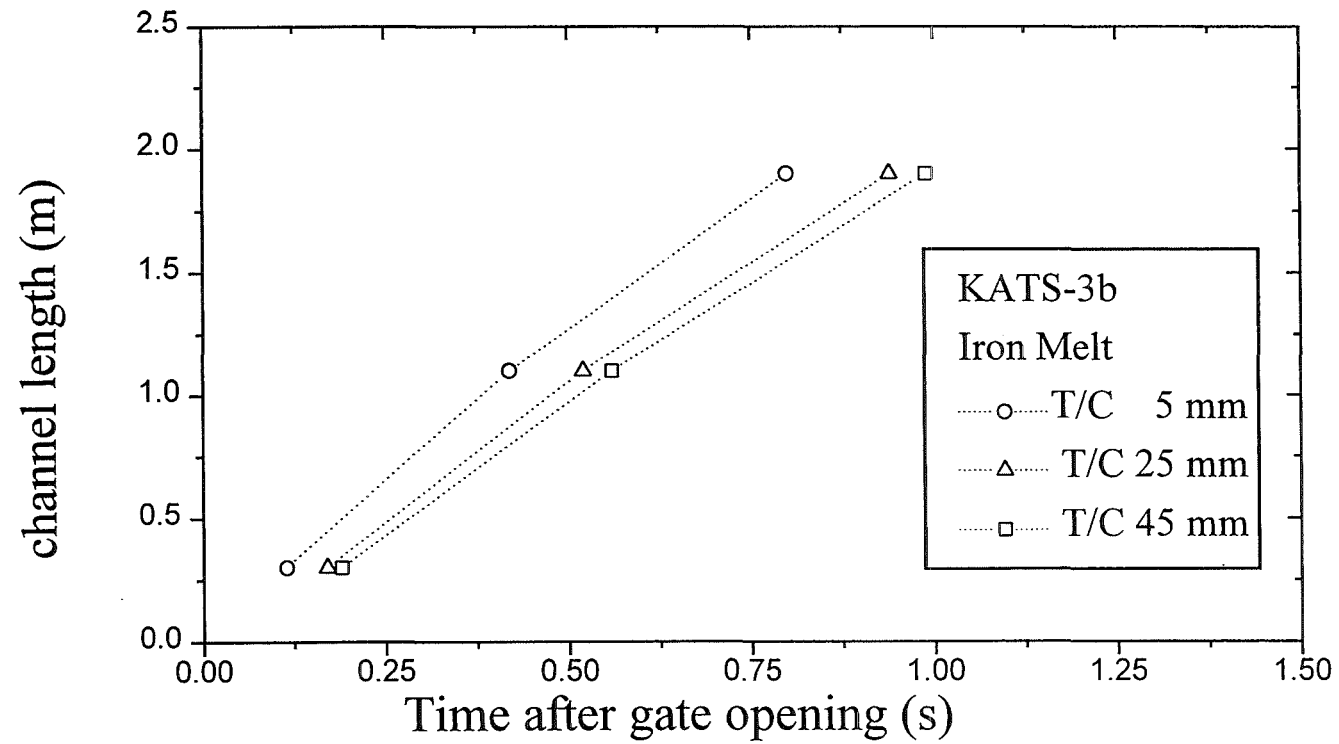
Fig. 12 Transient leading edge propagation of an iron melt into a short dry channel
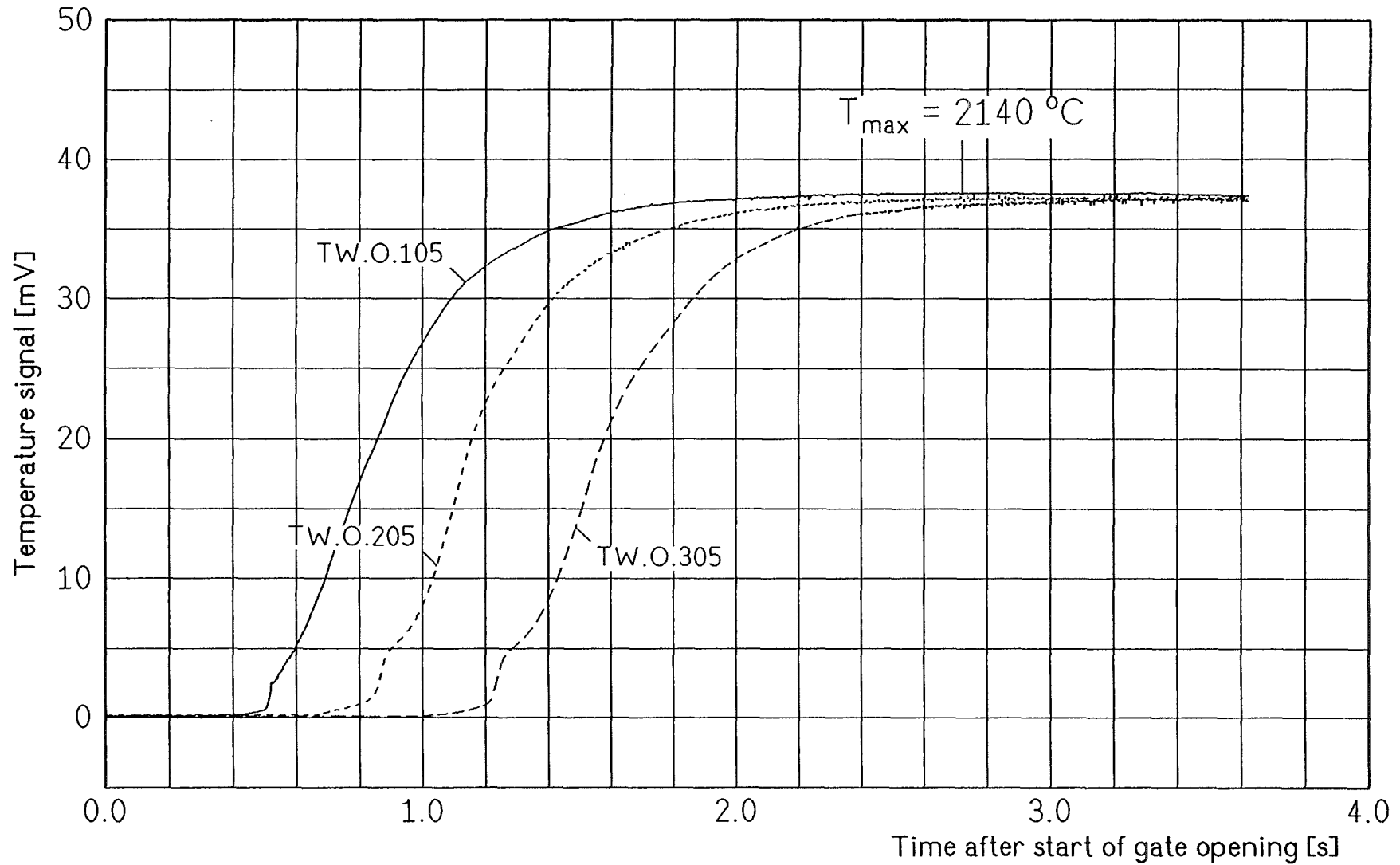
Fig. 13 Test KATS-3b   Temperature of the oxide melt at Pos.1/2/3
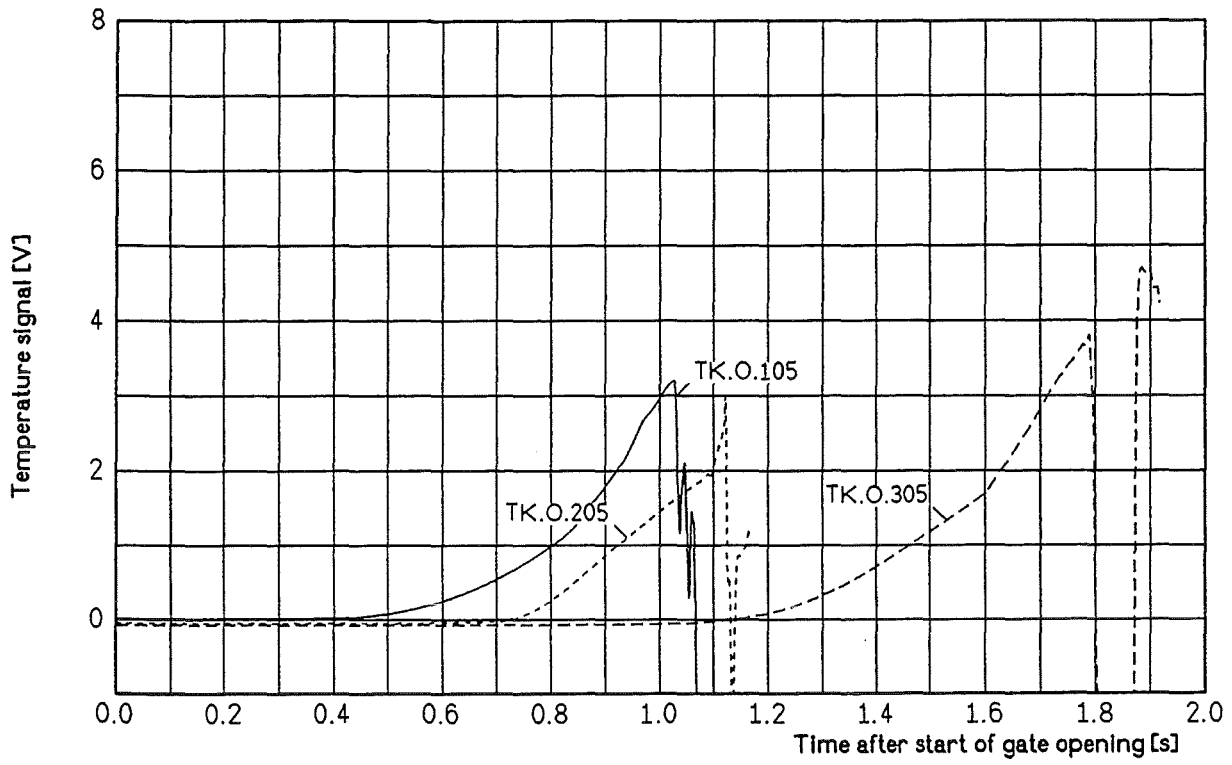
Fig.14 Test KATS-3b   Detection of the oxide melt at 5mm height
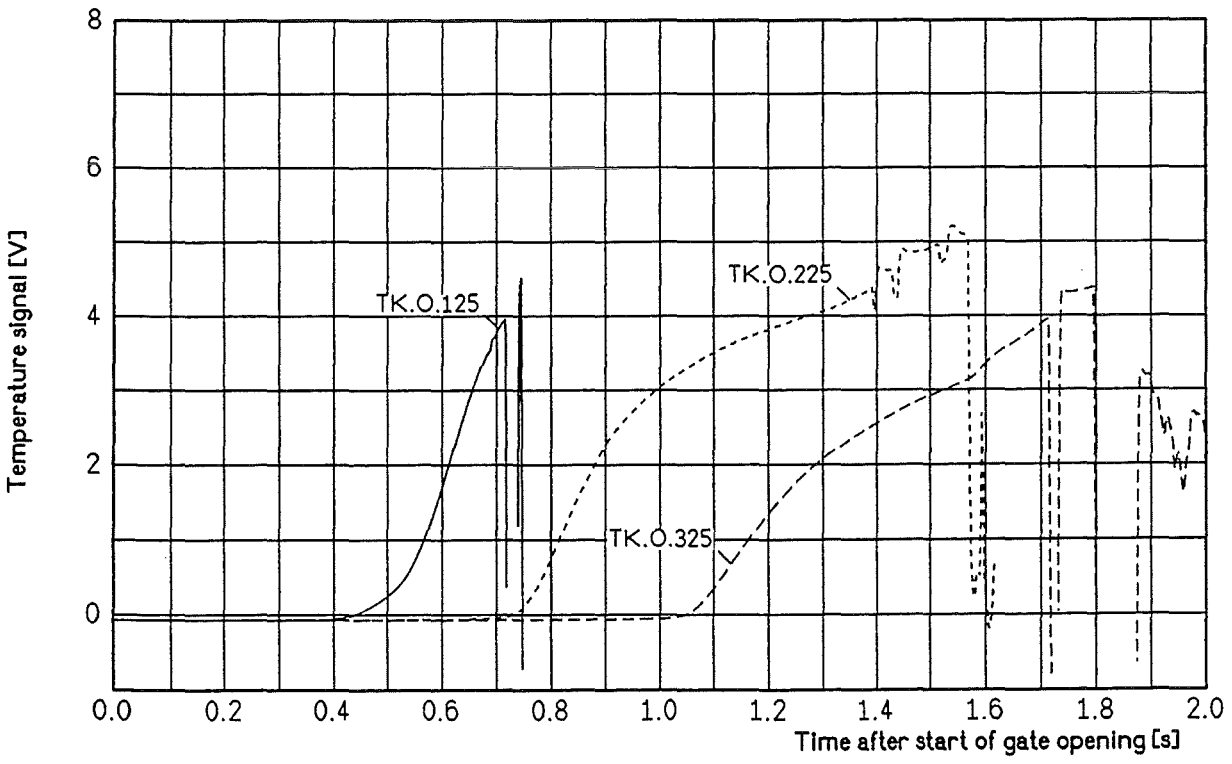
Fig. 15 Test KATS-3b   Detection of the oxide melt at 25mm height

29
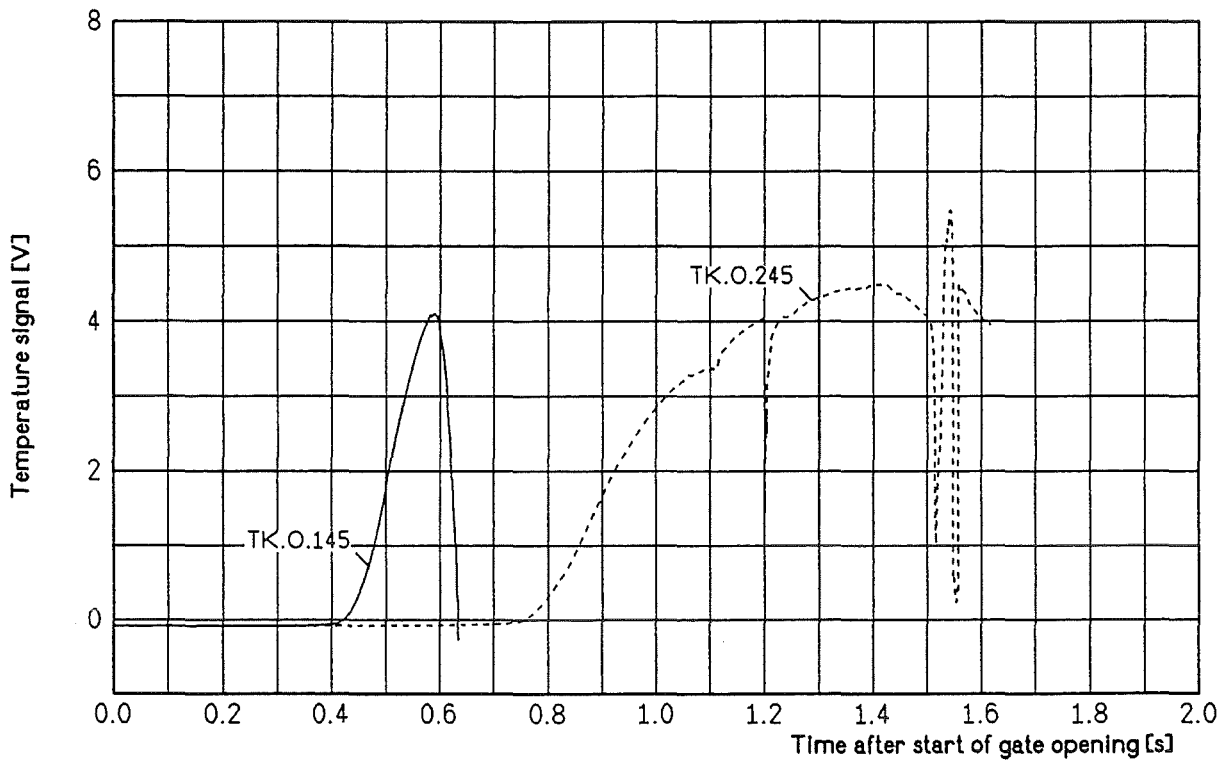
Fig.16　Test KATS-3b　　　Detection of the oxide melt at 45mm height
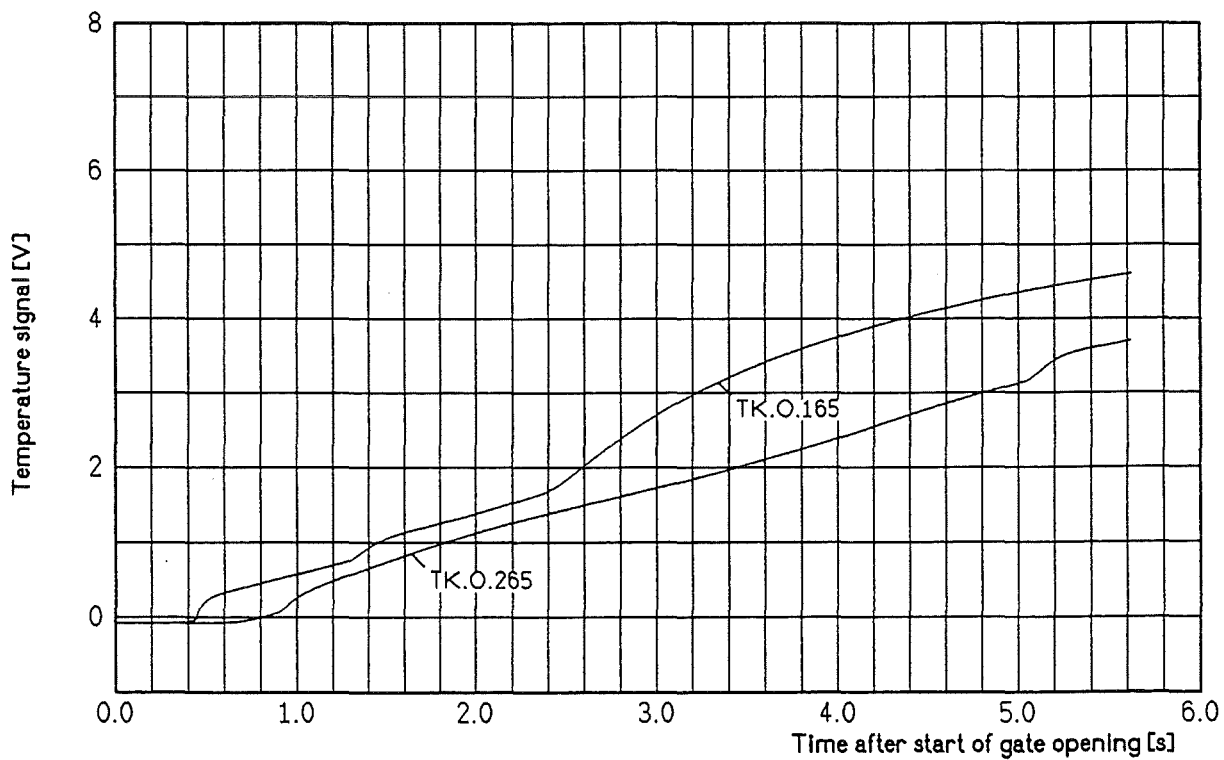
Fig. 17　Test KATS-3b　　　Detection of the oxide melt at 65mm height

30
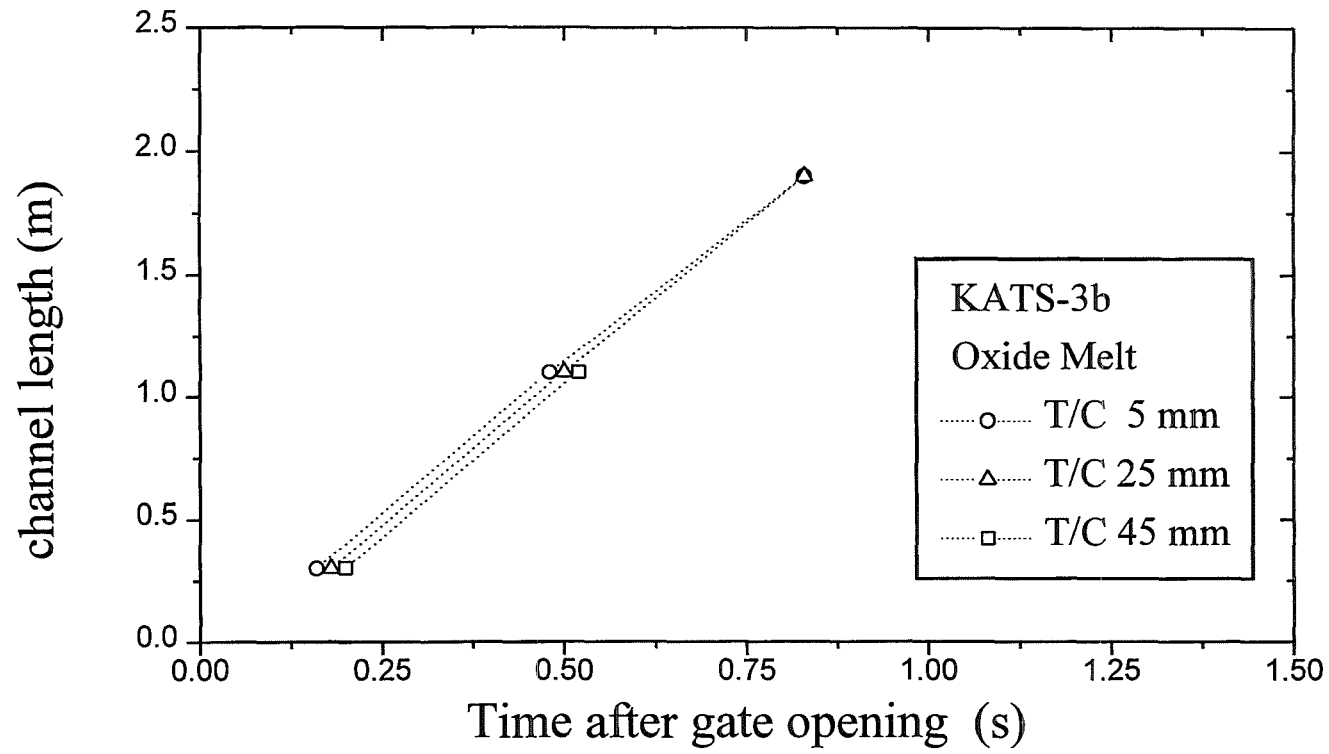
Fig.18 Transient leading edge propagation of an oxide melt into a short dry channel
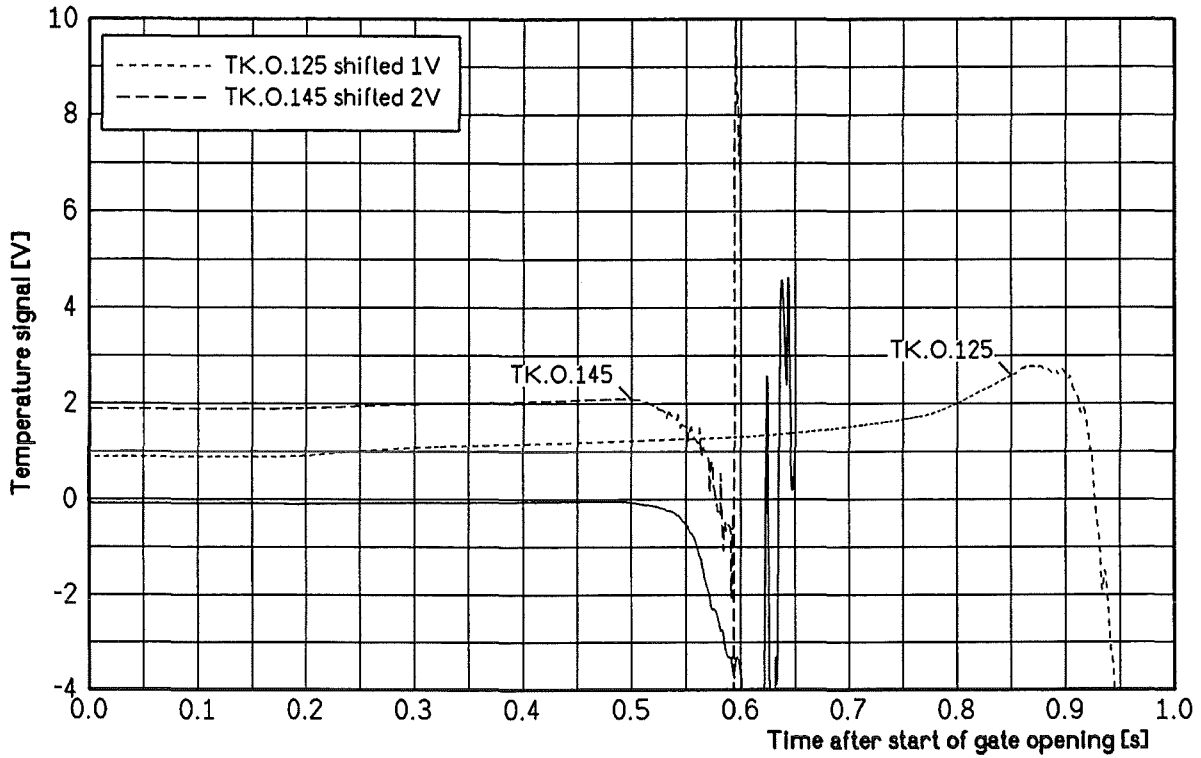
Fig.19 Test KATS-4   Detection of the oxide melt at Pos. 1
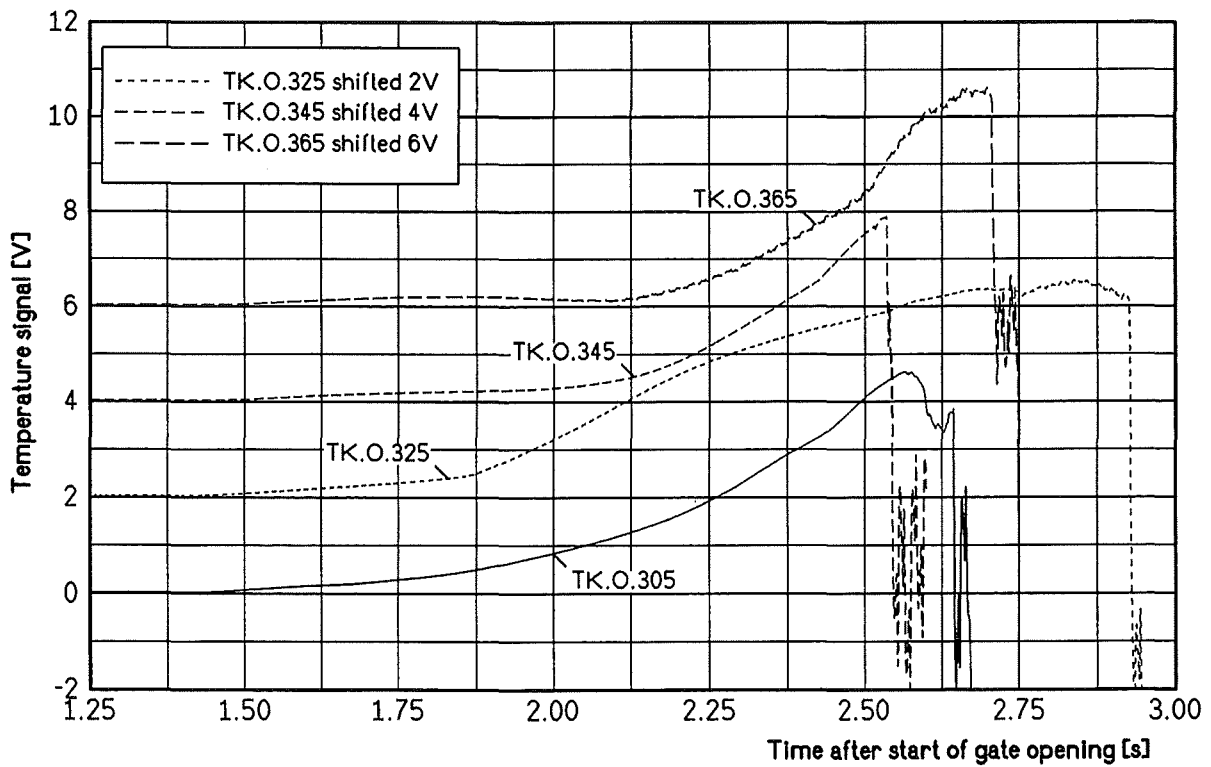
Fig.20 Test KATS-4   Detection of the oxide melt at Pos. 3

32
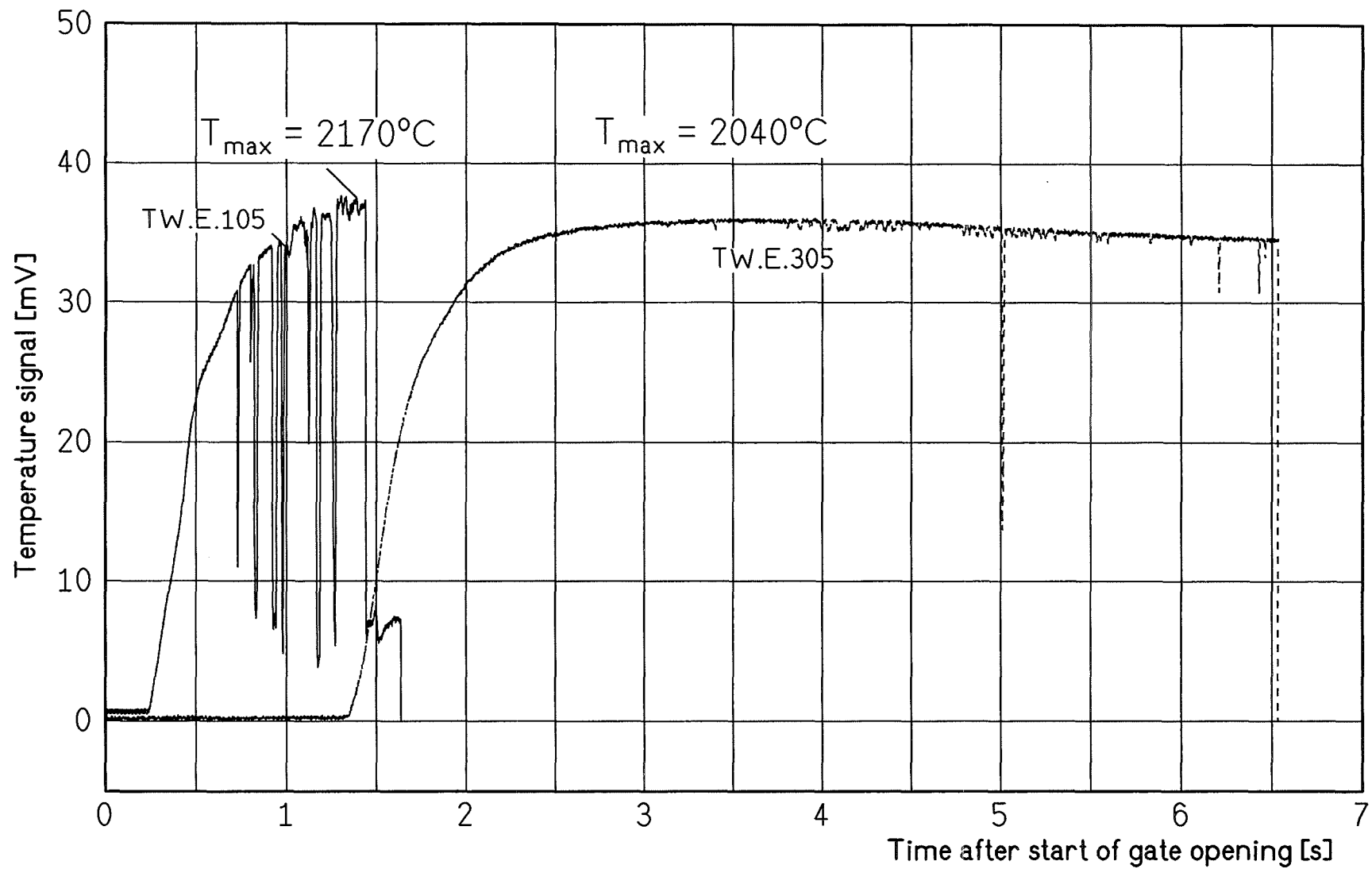
Fig. 21   Test KATS-4   Temperature of the iron melt at pos. 1/3
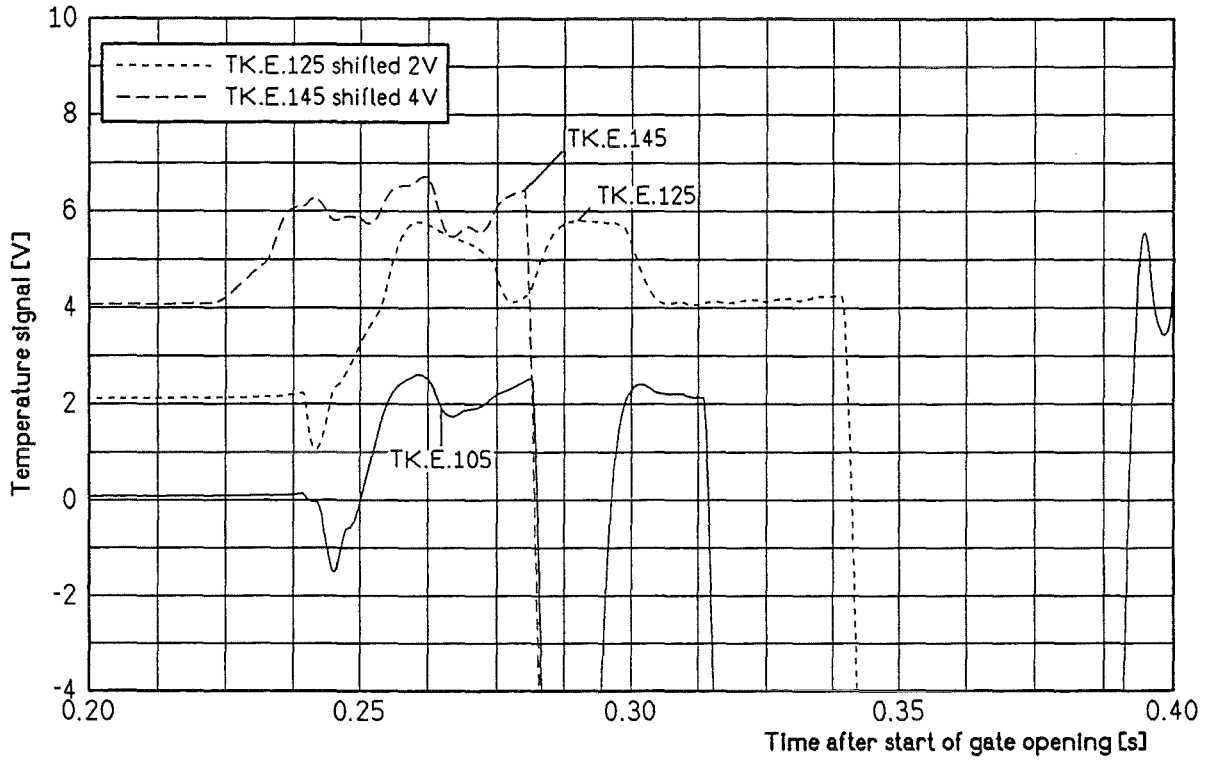
Fig.22 Test KATS-4　　　　　　　　Detection of the iron melt at Pos. 1
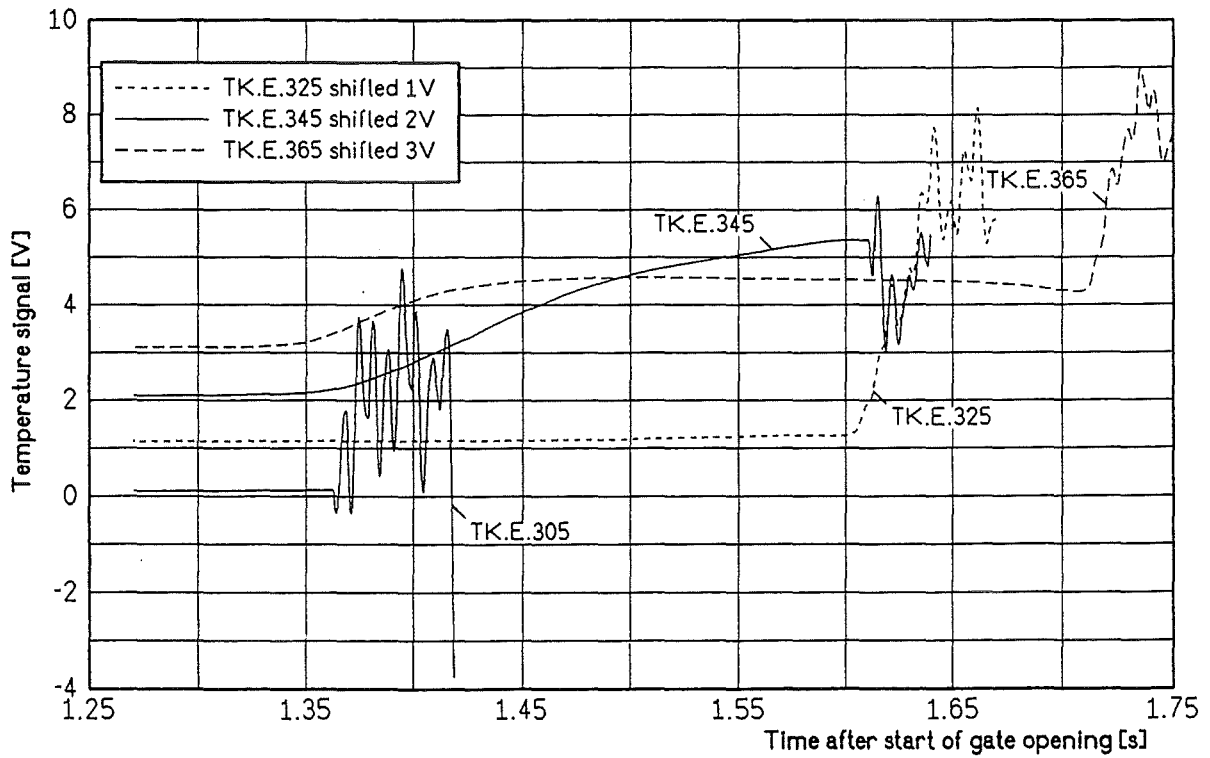
Fig.23 Test KATS-4　　　　　　　　Detection of the iron melt at Pos. 3

34